

4D ASR: Joint Beam Search Integrating CTC, Attention, Transducer, and Mask Predict Decoders

Yui Sudo, *Member, IEEE*, Muhammad Shakeel, *Member, IEEE*, Yosuke Fukumoto, *Non Member*, Brian Yan, *Student Member, IEEE*, Jiatong Shi, *Student Member, IEEE*, Yifan Peng, *Student Member, IEEE*, Shinji Watanabe, *Fellow, IEEE*,

Abstract—End-to-end automatic speech recognition (E2E-ASR) can be classified into several network architectures, such as connectionist temporal classification (CTC), recurrent neural network transducer (RNN-T), attention-based encoder-decoder, and mask-predict models. Each network architecture has advantages and disadvantages, leading practitioners to switch between these different models depending on application requirements. Instead of building separate models, we propose a joint modeling scheme where four decoders (CTC, RNN-T, attention, and mask-predict) share the same encoder – we refer to this as 4D modeling. The 4D model is trained using multitask learning, which will bring model regularization and maximize the model robustness thanks to their complementary properties. To efficiently train the 4D model, we introduce a two-stage training strategy that stabilizes multitask learning. In addition, we propose three novel one-pass beam search algorithms by combining three decoders (CTC, RNN-T, and attention) to further improve performance. These three beam search algorithms differ in which decoder is used as the primary decoder. We carefully evaluate the performance and computational tradeoffs associated with each algorithm. Experimental results demonstrate that the jointly trained 4D model outperforms the E2E-ASR models trained with only one individual decoder. Furthermore, we demonstrate that the proposed one-pass beam search algorithm outperforms the previously proposed CTC/attention decoding.

Index Terms—Speech recognition, CTC, attention-based encoder-decoder, RNN-T, beam search

I. INTRODUCTION

End-to-end automatic speech recognition (E2E-ASR) [1], [2] has been a subject of active research. Existing E2E-ASR systems include four main network architectures: connectionist temporal classification (CTC) [3]–[5], recurrent neural network transducer (RNN-T) [6]–[9], attention-based encoder-decoder [10]–[13], and non-autoregressive (NAR) methods [14]–[16]. These architectures align speech signals and token sequences in various ways, each with different strengths and weaknesses, as follows:

- CTC predicts a monotonic alignment of output tokens with input speech frames efficiently with the conditional independence assumption. While its parallelized inference across frames is fast, the conditional independence assumption results in suboptimal performance. CTC is also valuable for segmenting long recordings [17].

This paper was produced by the IEEE Publication Technology Group. They are in Piscataway, NJ.

Manuscript received May 23, 2024.

- RNN-T shares a monotonic alignment property with CTC but relaxes the conditional independence assumption. It typically outperforms CTC thanks to this relaxation and is particularly adept for streaming ASR [9]. However, due to its flexible alignment paths, its larger modeling space usually leads to additional training difficulties [18].
- Attention-based encoder-decoder employs a cross-attention mechanism to enable flexible alignments between input and output sequences, making it useful for various tasks such as translation [19], [20]. However, it may be susceptible to alignment errors in ASR tasks due to the lack of a monotonicity constraint [21].
- NAR methods, as exemplified by Mask-CTC [14], estimate the token sequence using the entire input sequence. The mask-based approach [22] maintains fast parallelized inference across frames, but unlike CTC, it accounts for label dependencies. It is also applicable in two-pass rescoring approaches for ASR error correction [23].

Owing to distinct characteristics in each network architecture, it is common to use corresponding models according to different application scenarios. For example, CTC is suitable for on-device systems with lower computational demands, whereas attention-based encoder-decoder is preferred for offline systems with less stringent latency requirements. However, maintaining multiple models for different application scenarios creates additional maintenance overhead for system administrators. Thus, several initiatives have attempted to integrate these models, such as hybrid CTC/attention, to mitigate their shortcomings [21], [24], [25]. The multitask learning in hybrid CTC/attention, achieved by sharing an encoder, helps to regularize the over-flexibility of the attention mechanism and the conditional independence assumption of the CTC model. During decoding, a one-pass beam search involving both CTC and attention decoders is employed to enhance performance further [21]. Such joint modeling has also been applied to large-scale E2E-ASR models [26]–[29]. Other integrated models, utilizing two-pass decoding of RNN-T/attention, NAR/attention, and RNN-T/NAR, have also been proposed [30]–[35]. These methods attempt to combine a streaming decoder with an offline decoder to achieve both low latency and high accuracy. In addition, several approaches have been explored to combine dual RNN-T models with different context lengths to optimize both latency and accuracy in ASR systems [36]–[41]. While integrating two of these models

has shown effectiveness, a more comprehensive integration of multiple models can exploit their complementary features to a greater extent. A single model can realize broader applications by minimizing the overhead of maintaining separate models.

In this study, we seek to jointly model four decoders (4D) with a shared encoder: CTC, attention, RNN-T, and Mask-CTC. The 4D model is trained using multitask learning, which will bring model regularization and maximize the model robustness thanks to their complementary properties. The jointly trained 4D model allows the selection of an appropriate decoder depending on different application scenarios. In addition, we propose three novel one-pass beam search algorithms using CTC, RNN-T, and attention to further enhance the complementarity of each decoder during inference.

The remainder of the manuscript is organized as follows: Section II describes the related work with a focus on the joint modeling of multiple decoders, highlighting the main contributions of this paper. Section III provides an overview of the four decoders, which are extended to the proposed 4D model in Section IV. Sections V and VI describe the experimental setup and results. Section VII discusses the practicality of the proposed method based on the experimental results, and Section VIII concludes the paper.

II. RELATED WORK

This section describes the joint modeling approach employing multiple decoders, especially in terms of the decoding approach. The joint decoding methods mainly fall into two categories: two-pass rescoring and one-pass beam search.

In the two-pass rescoring methods, the primary decoder generates complete hypotheses, followed by the other decoder rescoring those hypotheses to produce a more probable token sequence [30]–[35]. For example, in the two-pass rescoring of RNN-T/attention [30]–[32], the RNN-T decoder generates complete n-best hypotheses, and the attention decoder subsequently rescores them, leading to enhanced performance. However, the effectiveness of two-pass rescoring heavily relies on the first pass, because the second pass cannot correct the hypothesis unless the first pass contains the correct one [21].

Conversely, the one-pass beam search approach performs joint rescoring using the secondary decoder during the beam search process, without waiting for the primary decoder to complete hypothesis expansion. A typical example is the attention-driven one-pass beam search based on the hybrid CTC/attention [21]. In this method, the attention decoder serves as the primary decoder, and the CTC decoder scores the hypotheses generated by the attention decoder in a label-synchronous manner. This method integrates the two decoders more tightly, resulting in more accurate decoding than two-pass rescoring. This method has been extended to a CTC-driven one-pass beam search algorithm based on the CTC/attention architecture for speech translation tasks [42]. This method is computationally faster than the attention-driven one-pass beam search algorithm with almost comparable performance. Note that while both methods use the same CTC/attention architecture, the choice of primary decoder affects their performance and computational cost. Other method

includes the integration of time- and label-synchronous beam search using the streaming CTC/attention and the time-synchronous one-pass beam search using online/offline RNN-T decoders [43], [44].

While these methods have been successful with combinations of two decoders, there are still limited efforts in integrating three or more decoders. Additionally, only limited combinations of decoders have been considered for one-pass beam search (e.g., CTC/attention and online/offline RNN-T). Given that different primary decoders result in differences in performance and computational cost [42], a more comprehensive analysis is required.

Therefore, this paper proposes the 4D model consisting of CTC, attention, RNN-T, and Mask-CTC with a shared encoder. The jointly trained 4D model will bring model regularization and allow flexible choices of each decoder depending on different application scenarios. Furthermore, we introduce three novel one-pass beam search algorithms using CTC, RNN-T, and attention to enhance the complementarity of each decoder during inference. A comprehensive evaluation of the joint decoding is conducted by meticulously comparing the one-pass beam search algorithms of three different primary decoders. Specifically, we

- Demonstrate that each single-decoder of the 4D model is improved over counterparts without joint training with the efficient two-stage optimization strategy.
- Introduce novel one-pass beam search algorithms for joint CTC/RNN-T/attention decoding, showcasing superior performance on average compared to CTC/attention decoding.
- Analyze the effect of integrating multiple decoders in the beam search by carefully comparing the three one-pass beam search algorithms.

This paper extends our previous study on the 4D model [45] by newly proposing the attention-driven one-pass beam search for CTC/RNN-T/attention decoders (Section IV). We also analyze the effect of integrating multiple decoders by carefully comparing the three one-pass beam search algorithms including a more comprehensive set of experiments (Section VI). In addition, we provide detailed formulations of the four decoders (Section III).

III. PRELIMINARY

This section describes the conformer-based encoder, commonly used across the four network architectures: CTC, RNN-T, attention, and Mask-CTC. Subsequently, we provide a detailed description of each decoder.

A. Encoder

We adopt the conformer [13], [46] as the shared encoder in this study. The encoder comprises two convolutional layers and N conformer layers. The convolutional layers subsample a L -length audio feature sequence, $X = (\mathbf{x}_l \in \mathbb{R}^d | l = 1, \dots, L)$ into a $T(< L)$ -length subsampled feature sequence, $U = (\mathbf{u}_t \in \mathbb{R}^{d'} | t = 1, \dots, T)$, as follows:

$$U = \text{ConvSubsamp}(X). \quad (1)$$

Here, \mathbf{x}_t and \mathbf{u}_t are a d -dimensional speech feature vector (e.g., log Mel filterbanks) and d' -dimensional hidden state vector, respectively. Subsequently, the N conformer blocks transform the subsampled feature sequence U into a T -length hidden state sequence, $H = (\mathbf{h}_t \in \mathbb{R}^{d'} | t = 1, \dots, T)$, described as,

$$H = \text{Conformer}(U). \quad (2)$$

Each conformer block consists of a feed-forward layer (FFN), a multiheaded self-attention layer (MHSA), a convolution layer (Conv), and another FFN module, with layer normalization layers (LN) and residual connections [47], [48] as follows:

$$\tilde{U}_n = U_n + \frac{1}{2} \text{FFN}(\text{LN}(U_n)), \quad (3)$$

$$U'_n = \tilde{U}_n + \text{MHSA}(\text{LN}(\tilde{U}_n)), \quad (4)$$

$$U''_n = U'_n + \text{Conv}(\text{LN}(U'_n)), \quad (5)$$

$$U'''_n = U''_n + \frac{1}{2} \text{FFN}(\text{LN}(U''_n)), \quad (6)$$

where U_n and U'''_n represent the input and output of the n -th conformer block, respectively ($U_1 = U$ in Eq. (2)). Note that the LN layers are applied before each module followed by a residual connection as in [13]. By using N conformer blocks, the conformer encoder outputs the hidden state sequence ($H = U'''_N$).

The hidden state sequence H extracted by the encoder is fed into the decoder and the decoder estimates the S -length output token sequence, $Y = (y_s \in \mathcal{V} | s = 1, \dots, S)$, where \mathcal{V} and s represent the vocabulary and the label index, respectively. Each decoder is described in the following sections.

B. CTC

The CTC decoder predicts a T -length monotonic alignment sequence $Z_{\text{ctc}} = (z_t^{\text{ctc}} \in \mathcal{V} \cup \{\phi\} | t = 1, \dots, T)$ in a time-synchronous manner, where ϕ denotes a blank token. Each alignment sequence is deterministically mapped to a corresponding output sequence by removing all blank tokens ϕ and repetitive tokens defined by $\mathcal{B}_{\text{ctc}}(Z_{\text{ctc}}) = Y$ (e.g., $\mathcal{B}_{\text{ctc}}([a, a, \phi, a, \phi, b, b]) = [a, a, b]$). This mapping strategy constrains the efficient monotonic alignment. Note that the token sequence Y must be shorter than the T -length input sequence H . Instead of directly estimating output posteriors, $P(Y|X)$, the CTC decoder estimates the alignment posteriors, $P(Z_{\text{ctc}}|X)$ as follows:

$$P_{\text{ctc}}(Y | X) = \sum_{Z_{\text{ctc}} \in \mathcal{B}_{\text{ctc}}^{-1}(Y)} P(Z_{\text{ctc}} | X), \quad (7)$$

where $\mathcal{B}_{\text{ctc}}^{-1}(Y)$ is a set of all possible alignment sequences of Y as shown in Figure 1 (a). $P(Z_{\text{ctc}}|X)$ is computed by using a probabilistic chain rule and conditional independence assumption as follows:

$$P(Z_{\text{ctc}} | X) = \prod_{t=1}^T P(z_t^{\text{ctc}} | z_{1:t-1}^{\text{ctc}}, \mathbf{h}_t) \approx \prod_{t=1}^T P(z_t^{\text{ctc}} | \mathbf{h}_t), \quad (8)$$

where the previous alignment sequence $z_{1:t-1}^{\text{ctc}}$ is discarded based on the conditional independence assumption. While the

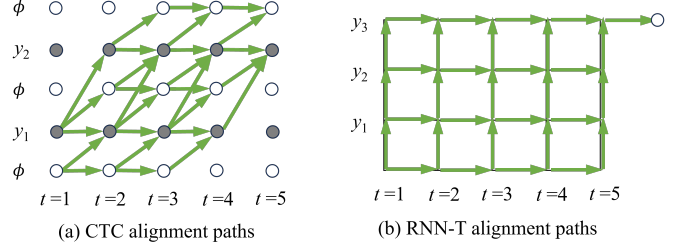


Fig. 1. Alignment paths of CTC and RNN-T. The CTC alignment path is of length T , while the RNN-T alignment path is of length $(T + S)$.

conditional independence assumption allows parallel computation, resulting in a fast inference, this architecture often leads to suboptimal performance due to the simplified dependencies between output labels.

Given H generated by the encoder in Eq. (2), the CTC decoder, typically consisting of a linear layer, estimates the alignment posterior as follows:

$$P(z_t^{\text{ctc}} | \mathbf{h}_t) = \text{Softmax}(\text{Linear}(\mathbf{h}_t)). \quad (9)$$

During training, CTC optimizes the model parameters by minimizing the negative log-likelihood as expressed below:

$$L_{\text{ctc}} = -\log P_{\text{ctc}}(Y | X). \quad (10)$$

C. RNN-T

Similar to the CTC decoder (Eq. (7)), the RNN-T decoder predicts a monotonic alignment sequence $Z_{\text{rnnnt}} = (z_i^{\text{rnnnt}} \in \mathcal{V} \cup \{\phi\} | i = 1, \dots, T + S)$ as follows:

$$P_{\text{rnnnt}}(Y | X) = \sum_{Z_{\text{rnnnt}} \in \mathcal{B}_{\text{rnnnt}}^{-1}(Y)} P(Z_{\text{rnnnt}} | X), \quad (11)$$

where $\mathcal{B}_{\text{rnnnt}}^{-1}(Y)$ is a set of all possible alignment sequences of Y (Figure 1 (b)). Each alignment sequence Z_{rnnnt} is deterministically mapped to a corresponding output sequence Y by removing all blank tokens defined by $\mathcal{B}_{\text{rnnnt}}(Z_{\text{rnnnt}}) = Y$. As with the CTC, this mapping strategy for RNN-T constrains the efficient monotonic alignment. However, unlike CTC which has conditional independence assumption in Eq. (8), the RNN-T decoder estimates $P(Z_{\text{rnnnt}} | X)$ considering the conditional dependency as follows:

$$P(Z_{\text{rnnnt}} | X) = \prod_{i=1}^{T+S} P(z_i^{\text{rnnnt}} | \mathbf{h}_t, y_{1:s-1}), \quad (12)$$

where t and s are determined by the alignment path z_i^{rnnnt} on the RNN-T lattice as shown in Figure 1 (b). Unlike CTC, the RNN-T alignment paths have length $(T + S)$, allowing a longer token sequence Y than the T -length input sequence H .

The RNN-T decoder typically comprises a prediction network and a joint network. The prediction network generates a high-level representation $\mathbf{g}_s \in \mathbb{R}^{d'}$ by conditioning on the previous non-blank token sequence $y_{1:s-1}$ with an embedding layer as follows:

$$\mathbf{g}_s = \text{PredNet}(\text{Embedding}(y_{1:s-1})). \quad (13)$$

The joint network estimates the alignment posterior z_i^{mnt} by combining \mathbf{h}_t (Eq. (2)) and \mathbf{g}_s (Eq. (13)) as follows:

$$P(z_i^{\text{mnt}} | \mathbf{h}_t, y_{1:s-1}) = \text{Softmax}(\text{JointNet}(\mathbf{h}_t, \mathbf{g}_s)). \quad (14)$$

RNN-T optimizes the model parameters by minimizing the negative log-likelihood as described below,

$$L_{\text{rnn}} = -\log P_{\text{rnn}}(Y | X). \quad (15)$$

D. Attention-based encoder-decoder

While CTC and RNN-T predict the alignment sequences (Eqs. (8) and (12)), the attention-based encoder-decoder directly estimates the posterior, $P_{\text{att}}(Y | X)$, in an autoregressive manner as follows:

$$P_{\text{att}}(Y | X) = \prod_{s=1}^S P(y_s | y_{1:s-1}, H). \quad (16)$$

Specifically, the token history $y_{1:s-1}$ is first converted to the token embeddings and fed into the M transformer blocks with the hidden state sequence H in Eq. (2). Then, $P(y_s | y_{1:s-1}, X)$ is calculated as follows:

$$\mathbf{r}_s = \text{Transformer}_s(\text{Embedding}(y_{1:s-1}), H), \quad (17)$$

$$P(y_s | y_{1:s-1}, X) = \text{Softmax}(\text{Linear}(\mathbf{r}_s)), \quad (18)$$

where $\mathbf{r}_s \in \mathbb{R}^{d'}$ represents the s -th hidden state vector.

Each transformer block in Eq. (17) comprises an MHSA layer, a multiheaded cross-attention layer (MHCA), and a FFN layer with LN layers and residual connections as follows:

$$V'_m = V_m + \text{MHSA}(\text{LN}(V_m)), \quad (19)$$

$$V''_m = V'_m + \text{MHCA}(\text{LN}(V'_m), H), \quad (20)$$

$$V'''_m = V''_m + \text{FFN}(\text{LN}(V''_m)), \quad (21)$$

where V_m and V'''_m represent the input and output of the m -th transformer block, respectively.

The MHCA in Eq. (20) is stacked cross-attention layers, and each cross-attention layer can be formulated as follows:

$$\text{CrossAttn}(V'_m, H) = \text{Softmax} \left(\frac{W^q V'_m (W^k H)^T}{\sqrt{d'}} \right) W^v H, \quad (22)$$

where W^q , W^k , and W^v represent the projection weight matrices for the query key, and vector, respectively. Here, the softmax term represents the alignment. Unlike CTC and RNN-T, which have reasonable monotonic alignment properties as discussed in Section III-B and III-C, the attention-based encoder-decoder does not maintain this constraint, which often provides irregular alignments.

Attention-based encoder-decoder optimizes the model parameters by minimizing the negative log-likelihood described as follows:

$$L_{\text{att}} = -\log P_{\text{att}}(Y | X). \quad (23)$$

E. Mask-CTC

Unlike the attention-based encoder-decoder model (Eq. (16)), the Mask CTC estimates the entire token sequence in a non-autoregressive manner based on a masked language model (MLM) [22]. Specifically, the MLM predicts a set of masked tokens y_{mask} conditioning on the hidden state sequence H in Eq. (2) and observed (unmasked) tokens y_{obs} as follows:

$$P_{\text{mlm}}(y_{\text{mask}} | y_{\text{obs}}, X) = \prod_{y \in y_{\text{mask}}} P(y | y_{\text{obs}}, H). \quad (24)$$

During training, randomly sampled tokens from the reference transcription are masked, while during inference, the low confidence tokens of the greedy CTC results are masked to generate y_{mask} .

Specifically, the observed tokens y_{obs} are first converted to the token embeddings and fed into the M transformer blocks with hidden state sequence H in Eq. (2) as follows:

$$r_{\text{mask}} = \text{Transformer}_{\text{mask}}(\text{Embedding}(y_{\text{obs}}), H), \quad (25)$$

$$P_{\text{mlm}}(y_{\text{mask}} | y_{\text{obs}}, X) = \text{Softmax}(\text{Linear}(r_{\text{mask}})), \quad (26)$$

where r_{mask} represents the hidden state vectors. Unlike the attention-based encoder-decoder model, the MLM predicts arbitrary subsets of masked tokens y_{mask} in a non-autoregressive manner. This mask-based approach maintains fast parallelized inference, but unlike CTC, it accounts for label dependencies.

Mask-CTC optimizes the model parameters by minimizing the following negative log-likelihood as follows:

$$L_{\text{mlm}} = -\log P_{\text{mlm}}(y_{\text{mask}} | y_{\text{obs}}, X). \quad (27)$$

IV. PROPOSED 4D ASR MODEL

This section describes the joint training process utilizing the two-stage optimization strategy and the beam search methodology employed in the proposed 4D model.

A. Joint training with a two-stage optimization strategy

Multitask learning is performed using the weighted sum of losses in Eqs. (10), (15), (23), and (27) described as follows:

$$L = \lambda_{\text{ctc}} L_{\text{ctc}} + \lambda_{\text{rnn}} L_{\text{rnn}} + \lambda_{\text{att}} L_{\text{att}} + \lambda_{\text{mlm}} L_{\text{mlm}}, \quad (28)$$

where $(\lambda_{\text{ctc}}, \lambda_{\text{rnn}}, \lambda_{\text{att}}, \lambda_{\text{mlm}})$ represent training weights. The training weights are usually determined experimentally [21] or based on meta-learning [49]. The complexity introduced by four weights makes conducting exhaustive experimental exploration impractical. To address this challenge, we implement a two-stage optimization strategy to determine the training weights. In the first stage, all four training weights are initialized to be equal (0.25, 0.25, 0.25, 0.25). Subsequently, in the second stage, these weights are proportionally adjusted based on the epochs at which each validation loss reaches its minimum value in the first stage. For example, if the validation losses ($L_{\text{ctc}}, L_{\text{rnn}}, L_{\text{att}}, L_{\text{mlm}}$) reach their minimum values at the 10th, 10th, 10th, and 70th epochs in the first stage, the training weights in the second stage are set to (0.1, 0.1, 0.1, 0.7). This strategy is based on the proposition that losses requiring more epochs to converge should be given higher weights.

B. Overview of the joint decoding of CTC/RNN-T/attention

Another contribution of this paper is the introduction of three one-pass beam search algorithms using CTC/RNN-T/attention decoders: attention-driven, CTC-driven, and RNN-T-driven one-pass beam search. The proposed one-pass beam search algorithms consist of three parts: hypotheses expansion using a primary decoder, joint scoring using the other two decoders, and beam pruning based on the joint score. The difference between the three one-pass beam search algorithms is based on which decoder is the primary decoder. Subsequent sections delve into the specifics of the three variants of the proposed one-pass beam search algorithms.

Note that, the Mask-CTC is excluded from the proposed beam search because it predicts the entire output sequence in parallel, unlike the other three decoders.

C. Attention-driven one-pass beam search

In the attention-driven one-pass beam search, the attention decoder serves as the primary decoder to generate hypotheses whose scores are augmented by the CTC decoder and the RNN-T decoder as shown in Algorithm 1. This approach directly extends the joint CTC/attention decoding algorithm proposed in [21], including RNN-T scoring.

1) *Overall flow*: Similar to the joint CTC/attention decoding, the attention decoder primarily generates k_{pre} hypotheses (ext_hyps) with the scores α_{att} label-synchronously (lines 5-10 in Algorithm 1), where k_{pre} represents the pre-beam size, which is larger than the main beam size k_{beam} . Subsequently, each hypothesis \tilde{l} in ext_hyps is scored using the CTC and RNN-T decoders (lines 13-14 in Algorithm 1). The CTC score α_{ctc} is computed using the CTC prefix scoring as in [21]. Similarly, we propose the RNN-T prefix scoring to calculate the RNN-T score α_{rnn} label-synchronously, which will be described in Section IV-C2. Each score is then added using the decoder weights (μ_{ctc} , μ_{att} , μ_{rnn}) along with the length penalty β (line 16 in Algorithm 1). After that, if $y_s = \text{<eos>}$, the hypothesis \tilde{l} is assumed to be complete and stored in end_hyps (line 18 in Algorithm 1). Otherwise, \tilde{l} is stored in ext_hyps with the joint score α_{joint} (line 20 in Algorithm 1). Finally, the top k_{beam} hypotheses (hyps) are retained for the next label frame based on the joint score α_{joint} (line 22 in Algorithm 1).

2) *RNN-T prefix scoring*: Similar to the CTC prefix scoring [21] in joint CTC/attention decoding, we propose the RNN-T prefix scoring, which modifies a forward algorithm in a label synchronous manner. Algorithm 2 shows the details of the RNN-T prefix scoring, which computes the sum of the probabilities of all RNN-T paths that yield the hypothesis \tilde{l} . Specifically, it repeats the $\gamma_t(l)$ computation step and the $\Psi_t(\tilde{l})$ computation step (lines 3-4 in Algorithm 2). Here, $\gamma_t(l)$ and $\Psi_t(\tilde{l})$ denote the sum of the probabilities yielding hypothesis l and the probability of outputting the last token y_s , resulting in the hypothesis \tilde{l} at time t , respectively (Figure 2).

First, $\gamma_t(l)$ is computed based on $\Psi_t(l)$, which is initialized for $t = 1, \dots, T$ before starting the beam search (line 2 in Algorithm 1). As depicted in Figure 2 (a), $\gamma_t(l)$ is the sum of $\Psi_t(l)$ and the probability of outputting a blank label ϕ from $\gamma_{t-1}(l)$. Then, $\Psi_t(\tilde{l})$ is computed using $\gamma_t(l)$ (line

Algorithm 1 Attention-driven one-pass beam search

```

1:  $\text{hyps} = \{\text{sos}:1.0\}; \text{end\_hyps} = \{\}$ 
2:  $\Psi_t(\text{sos}) = \begin{cases} 1 & (t = 1) \\ 0 & (\text{otherwise}) \end{cases}$ 
3: for  $s = 1$  to  $S_{\text{max}}$  do
4:    $\text{ext\_hyps} = \{\}$ 
5:   for  $\tilde{l} \in \text{hyps}$  do Hypothesis expansion (attention)
6:     for  $y_s \in \text{top-}k_{\text{pre}}(P(y_s | \tilde{l}, H))$  do
7:        $\tilde{l} = \tilde{l} \oplus y_s$ 
8:       Add  $\tilde{l}$  and score  $\alpha_{\text{att}} = P_{\text{att}}(\tilde{l} | X)$  to  $\text{ext\_hyps}$ 
9:     end for
10:   end for
11:   for  $\tilde{l} \in \text{ext\_hyps}$  do Joint scoring (CTC/RNN-T)
12:      $\alpha_{\text{att}} = \text{ext\_hyps}[\tilde{l}]$ 
13:      $\alpha_{\text{ctc}} = \text{CTCPrefixScore}(\tilde{l}, H)$ 
14:      $\alpha_{\text{rnn}}, \Psi_t(\tilde{l}) = \text{RNNTPrefixScore}(\tilde{l}, H, \Psi_t(l))$ 
15:      $\beta = \text{LengthPenalty}(\tilde{l})$ 
16:      $\alpha_{\text{joint}} = \mu_{\text{ctc}} \alpha_{\text{ctc}} + \mu_{\text{att}} \alpha_{\text{att}} + \mu_{\text{rnn}} \alpha_{\text{rnn}} + \beta$ 
17:     if  $(y_s = \text{<eos>})$  then
18:       Add  $\tilde{l}$  and score  $\alpha_{\text{joint}}$  to  $\text{end\_hyps}$ 
19:     else
20:        $\text{ext\_hyps}[\tilde{l}] = \alpha_{\text{joint}}$ 
21:     end if
22:    $\text{hyps} = \text{top-}k_{\text{beam}}(\text{ext\_hyps})$  Beam pruning
23:   end for
24: end for
25: return  $\text{end\_hyps}$ 

```

Algorithm 2 RNN-prefix scoring

```

1:  $l, y_s \leftarrow \tilde{l}$  (split  $\tilde{l}$  into the last token  $y_s$  and the rest  $l$ )
2: for  $t = 1$  to  $T$  do
3:    $\gamma_t(l) = \begin{cases} \Psi_t(l) & (t = 1) \\ \Psi_t(l) + \gamma_{t-1}(l) + P(\phi | \mathbf{h}_{t-1}, l) & (t > 1) \end{cases}$ 
4:    $\Psi_t(\tilde{l}) = \gamma_t(l) P(y_s | \mathbf{h}_t, l)$ 
5: end for
6: If  $y_s = \text{<eos>}$  then
7:    $\alpha_{\text{rnn}} = \gamma_T(l) P(\phi | \mathbf{h}_T, l)$ 
8: else
9:    $\alpha_{\text{rnn}} = \sum_{t=1}^T \Psi_t(\tilde{l})$ 
10: end if
11: return  $\alpha_{\text{rnn}}, \Psi_t(\tilde{l})$ 

```

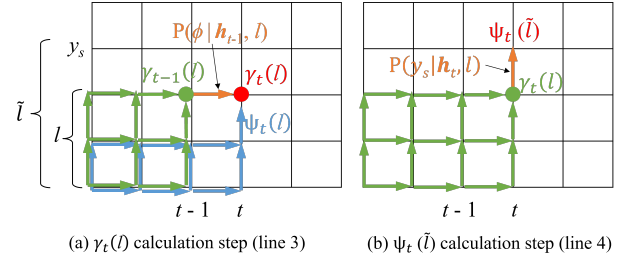


Fig. 2. RNN-T prefix scoring (lines 3 and 4 in Algorithm 2).

4 in Algorithm 2). As shown in Figure 2 (b), $\Psi_t(\tilde{l})$ is the probability of outputting y_s from $\gamma_t(l)$. These processes are computed iteratively for $t = 1, \dots, T$. Finally, $\Psi_t(\tilde{l})$ is summed for $t = 1, \dots, T$ (line 9 in Algorithm 2). If y_s is the <eos> token, the probability of outputting a blank label ϕ at time T is determined from $\gamma_T(l)$ (line 7 in Algorithm 2).

Algorithm 3 CTC-driven one-pass beam search

```

1:  $hyp = \{\text{<sos>:1.0}\}; ext\_hyp = \{\}$ 
2:  $\Psi_t(\text{<sos>}) = \begin{cases} 1 & (t = 1) \\ 0 & (\text{otherwise}) \end{cases}$ 
3: for  $t = 1$  to  $T$  do
4:   for  $l \in hyps$  do Hypothesis expansion
5:     for  $z_t \in \text{top-}k_{\text{pre}}(P(z_t | h_t))$  do
6:        $\tilde{l} = l \oplus z_t$  ( $\text{if } z_t \text{ is not } \phi \text{ else } \tilde{l} = l$ ) (CTC)
7:       Add  $\tilde{l}$  and score  $\alpha_{\text{ctc}} = P_{\text{ctc}}(\tilde{l} | X)$  to  $ext\_hyp$ 
8:     end for
9:   end for
10:  for  $\tilde{l} \in ext\_hyp$  do Joint scoring (attention/RNN-T)
11:     $\alpha_{\text{ctc}} = ext\_hyp[\tilde{l}]$ 
12:     $\alpha_{\text{att}} = \text{AttScore}(\tilde{l}, H)$ 
13:     $\alpha_{\text{rnnnt}}, \Psi_t(\tilde{l}) = \text{RNNTPrefixScore}(\tilde{l}, H, \Psi_t(l))$ 
14:     $\beta = \text{LengthPenalty}(\tilde{l})$ 
15:     $ext\_hyp[\tilde{l}] = \mu_{\text{ctc}} \alpha_{\text{ctc}} + \mu_{\text{att}} \alpha_{\text{att}} + \mu_{\text{rnnnt}} \alpha_{\text{rnnnt}} + \beta$ 
16:  end for
17:   $hyp = \text{top-}k_{\text{beam}}(ext\_hyp)$  Beam pruning
18: end for
19: return  $hyp$ 

```

Note that CTC prefix scoring and RNN-T prefix scoring require more computation for scoring than using the CTC and RNN-T decoders as the primary decoder, respectively, because all possible CTC and RNN-T alignment paths must be computed.

D. CTC-driven one-pass beam search

The CTC-driven one-pass beam search employs the CTC decoder as the primary decoder, and the scores of the hypotheses generated by the CTC decoder are augmented by the attention decoder and the RNN-T decoder. This approach is similar to CTC-driven beam search with the attention decoder [42], [50], but with an additional consideration of RNN-T likelihoods.

As shown in Algorithm 3, the CTC decoder generates the k_{pre} hypotheses with the CTC score α_{ctc} , denoted as ext_hyp (lines 4-9 in Algorithm 3). Subsequently, the generated hypotheses, ext_hyp , are scored using the attention and RNN-T decoders (lines 12-13 in Algorithm 3). The attention score α_{att} is computed using the forward computation as described in Eq. (16). Similar to the attention-driven one-pass beam search (in Algorithm 1), the RNN-T prefix scoring is used to compute the RNN-T score α_{rnnnt} . Note that although both CTC and RNN-T are based on time-synchronous beam search, they have different alignment paths and different mapping functions, as shown in Figure 1. Since the CTC alignment path cannot be directly scored by the RNN-T decoder, the RNN-T prefix scoring is used after all blank labels are removed. Each decoder score is then added using the decoder weights ($\mu_{\text{ctc}}, \mu_{\text{att}}, \mu_{\text{rnnnt}}$) along with the length penalty (line 15 in Algorithm 3). Finally, the top k_{beam} hypotheses, hyp , are retained for the next time frame based on the joint score (line 17 in Algorithm 3). Unlike the attention-driven one-pass beam search, this process is iterated time-synchronously ($t = 1, \dots, T$).

Algorithm 4 RNN-T-driven one-pass beam search

```

1:  $hyp = \{\text{<blank>:1.0}\}$ 
2: for  $t = 1$  to  $T$  do
3:    $A = hyps; ext\_hyp = \{\}$ 
4:   while  $ext\_hyp$  contains less than  $k_{\text{pre}}$  hypotheses more probable than the most probable in  $A$  do
5:      $l = \text{most probable in } A; \text{remove } l \text{ from } A$ 
6:     Add  $l$  and score  $\alpha_{\text{rnnnt}} = A[l] \cdot P(\phi | h_t, l)$  to  $ext\_hyp$ 
7:     for  $z_t \in \text{top-}k_{\text{pre}}(P(z_t | h_t, l))$  do
8:       Add  $l \oplus z_t$  and score  $\alpha_{\text{rnnnt}} = A[l] \cdot P(z_t | h_t, l)$  to  $A$  Hypothesis expansion (RNN-T)
9:     end for
10:    for  $\tilde{l} \in ext\_hyp$  do Joint scoring (attention/RNN-T)
11:       $\alpha_{\text{rnnnt}} = ext\_hyp[\tilde{l}]$ 
12:       $\alpha_{\text{att}} = \text{AttScore}(\tilde{l}, H)$ 
13:       $\alpha_{\text{ctc}} = \text{CTCPrefixScore}(\tilde{l}, H)$ 
14:       $\beta = \text{LengthPenalty}(\tilde{l})$ 
15:       $ext\_hyp[\tilde{l}] = \mu_{\text{ctc}} \alpha_{\text{ctc}} + \mu_{\text{att}} \alpha_{\text{att}} + \mu_{\text{rnnnt}} \alpha_{\text{rnnnt}} + \beta$ 
16:    end for
17:     $hyp = \text{top-}k_{\text{beam}}(ext\_hyp)$  Beam pruning
18:  end for
19:  return  $hyp$ 

```

Note that while the CTC-driven one-pass beam search algorithm avoids CTC prefix scoring which calculates all possible CTC alignment paths, it still computes all possible RNN-T alignment paths via RNN-TPrefixScore(\cdot).

E. RNN-T-driven one-pass beam search

The RNN-T-driven one-pass beam search employs the RNN-T decoder as the primary decoder, and the scores of the hypotheses generated by the RNN-T decoder are augmented by the CTC decoder and attention decoder. Unlike the two-pass rescoring-based methods [30], [32]–[35], the joint scoring is performed time-synchronously in the one-pass beam search.

First, the RNN-T decoder generates the k_{pre} hypotheses (lines 4-9 in Algorithm 4). Subsequently, the generated hypotheses, ext_hyp , are scored by combining the CTC and attention decoders (lines 12-13 in Algorithm 4). The attention score is calculated using the forward computation as in Eq. (16). The CTC score is calculated using CTC prefix scoring as in [21]. Note that although both CTC and RNN-T are based on time-synchronous beam search, they have different alignment paths and different mapping functions, as shown in Figure 1. Since the RNN-T alignment path cannot be directly scored by the CTC decoder, the CTC prefix scoring is used after all blank labels are removed. Each decoder score is then added using the decoder weights ($\mu_{\text{ctc}}, \mu_{\text{att}}, \mu_{\text{rnnnt}}$) along with the length penalty (line 15 in Algorithm 4). Finally, the top k_{beam} hypotheses, hyp , are retained for the next time frame based on the obtained joint score (line 17 in Algorithm 4). Similar to the CTC-driven one-pass beam search, this process is repeated time-synchronously ($t = 1, \dots, T$).

Note that the RNN-T-driven one-pass beam search algorithm avoids RNN-T prefix scoring which computes all RNN-T alignment paths unlike the other two one-pass beam search algorithms (Section IV-C and IV-D).

TABLE I

COMPARISON OF THE 4D MODELS (B1-8) AGAINST RESPECTIVE BASELINES (A1-5). THE BEST WER/CER (\downarrow) RESULT IN EACH COMPARISON IS **BOLDED**, AND THE BEST RESULTS OVERALL ARE FURTHER UNDERLINED. THE AVERAGE ABSOLUTE IMPROVEMENTS (Δ) ARE ALSO SHOWN.

ID	Model Name	4D joint training	Proposed beam search	LibriSpeech 960 h		LibriSpeech 100 h		In-house (855 h)		
				test-clean	test-other	test-clean	test-other	assembly	meeting	avg Δ
A1	Attention	-	-	2.88	5.62	8.59	19.43	3.81	5.82	-
B1	4D (Attention)	yes	-	2.66	5.62	7.83	17.91	3.56	5.31	-0.54
A2	CTC	-	-	3.10	6.90	8.20	20.66	3.91	6.30	-
B2	4D (CTC)	yes	-	2.84	6.39	7.30	18.96	3.74	5.53	-0.72
A3	Mask-CTC	-	-	2.97	6.92	8.72	20.78	4.37	6.56	-
B3	4D (Mask-CTC)	yes	-	3.11	6.82	7.47	18.97	3.86	6.24	-0.64
A4	RNN-T	-	-	2.66	5.82	7.25	18.30	4.00	5.91	-
B4	4D (RNN-T)	yes	-	2.56	5.74	7.10	17.61	3.94	5.30	-0.28
A5	CTC/Attention	-	-	2.45	5.18	7.08	17.80	3.75	5.72	-
B5	4D (CTC/Attention)	yes	-	2.42	5.31	6.49	17.03	3.67	5.17	-0.32
A5	CTC/Attention	-	-	2.45	5.18	7.08	17.80	3.75	5.72	-
B6	4D (CTC/RNN-T/Attn)	yes	Attn-driven	2.45	5.32	6.54	16.65	3.72	5.12	-0.36
B7	4D (CTC/RNN-T/Attn)	yes	CTC-driven	2.36	5.27	6.25	16.76	3.68	5.14	-0.42
B8	4D (CTC/RNN-T/Attn)	yes	RNN-T-driven	2.38	5.21	6.33	16.43	3.65	5.16	-0.47

V. EXPERIMENTAL SETUP

To evaluate the effectiveness of the proposed method, the 4D model is trained and evaluated using several datasets described below.

A. Model

The input features are 80-dimensional Mel-scale filter-bank features with a window size of 512 samples and a hop length of 160 samples. The sampling frequency is 16 kHz. Then, SpecAugment [51] is applied. The conformer encoder comprises two convolutional layers with a stride of two, a 512-dimensional linear projection layer, and 12 conformer blocks with 2048 linear units, each incorporating layer normalization with residual connections. The CTC decoder is a linear layer. The attention and MLM decoders have six transformer blocks, each with 2048 linear units. The attention dimension size is 512, with an eight-multihead attention mechanism. The RNN-T decoder employs a long short-term memory (LSTM) with a hidden size of 512 and a linear layer of 640 joint sizes for the prediction and joint networks, respectively.

The proposed model is trained for 150 epochs using the Adam optimizer [52] at a learning rate of 0.0015, with 150000 warmup steps. The training weights (λ_{ctc} , λ_{rnn} , λ_{att} , λ_{mlm}) of the second stage are (0.15, 0.10, 0.30, 0.45) based on the two-stage optimization strategy described in Section IV-A, which will be discussed in Section VI-B. The decoder weights (μ_{ctc} , μ_{rnn} , μ_{att}) of the attention-driven, CTC-driven, and RNN-T-driven beam search in Algorithms 1, 3, and 4 are (0.2, 0.2, 0.6), (0.3, 0.3, 0.4), and (0.1, 0.4, 0.5), respectively. The main beam size k_{beam} and prebeam size k_{pre} are 20 and 30, respectively.

B. Dataset

The proposed method is tested using the LibriSpeech (960 h, 100 h) [53] and our in-house dataset. Our in-house dataset¹ comprises 93 hours of Japanese speech data, collected from various scenarios such as meetings and morning assemblies, in addition to 581 hours of the Corpus of Spontaneous Japanese [54] and 181 hours of Japanese speech database

developed by the Advanced Telecommunications Research Institute International (ATR-APP) [55]. The word/character error rates (WER/CER) are calculated for the LibriSpeech and our in-house dataset using the ESPnet [56] toolkit.

VI. RESULTS

In this section, we first discuss the main results of the proposed method in Section VI-A. Subsequently, we explore the effectiveness of both joint training and decoding in Section VI-B and VI-C. Finally, we thoroughly compare the three proposed one-pass beam search algorithms in Section VI-D.

A. Main results

Table I presents a comprehensive overview of the results, evaluating the effect of both joint training and decoding strategies. First, we observe that the individual decoder branches of the 4D model exhibit superior performance compared to their non-4D trained counterparts (A1-4 vs. B1-4). Specifically, the 4D model enhances the CTC, attention, RNN-T, and Mask-CTC models, resulting in an overall improvement of 0.28-0.72 WER/CER. This improvement also holds for the CTC/attention models, as demonstrated by the comparison between A5 and B5. The results confirm that joint training significantly contributes to the enhanced performance of the individual decoders.

Beyond joint training, Table I also shows the results of the three proposed one-pass beam search algorithms. These methods consistently outperform the CTC/attention baseline, as indicated by the improvements seen in A5 compared to B6-8. In particular, the RNN-T-driven CTC/RNN-T/attention decoding shows a better performance improvement (an average of 0.47 WER/CER improvement) than the other two one-pass beam search methods. Notably, these improvements are more pronounced on the LibriSpeech 100 h dataset, suggesting that the 4D approach provides a regularization effect that is particularly beneficial when training data are limited.

B. Detailed analysis of the joint training

This section provides a detailed analysis of joint training. The subsequent subsections examine the proposed two-stage

¹Our in-house dataset is not released for privacy and confidentiality reasons.

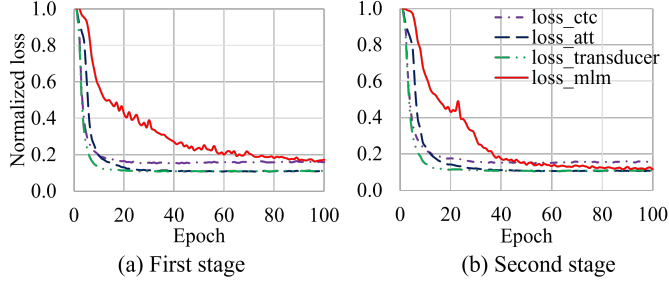


Fig. 3. Validation curves of the first vs. second training stage.

TABLE II
EFFECT OF THE TWO-STAGE TRAINING WITH LIBRISPEECH 100 H.

Decoder	WER (↓)		
	Non-4D	1st stage	2nd stage
Attention	19.43	18.69	17.91
CTC	20.66	19.52	18.96
Mask-CTC	20.78	20.38	18.97
RNN-T	18.30	18.10	17.61

training, the effect of the number of decoders in joint training, and the training time.

1) *Analysis of the two-stage training strategy*: Figure 3 illustrates the normalized validation losses in the first and second training stages. Note that the validation losses are normalized for a comparative analysis of convergence speed rather than focusing on the magnitude of the losses. During the first training stage (Figure 3 (a)), the MLM loss exhibits relatively slower convergence, suggesting potential under-convergence with the MLM decoder or potential overfitting with the other decoders. However, in the second training stage (Figure 3 (b)), the gap in convergence speed among the four losses decreases, indicating a more balanced convergence across all decoders.

Table II presents the performance of each decoder on the test-other set of LibriSpeech 100 h without and with 4D joint training in the first and second stages. Even in the first stage, where each model outperforms the performance of the non-4D multitask learning model, all four decoders exhibit improved performance in the second stage. This indicates the effectiveness of the proposed two-stage approach in efficiently determining the four weights through only two experimental trials.

2) *Effect of the number of decoders*: Table III depicts the relationship between the number of decoders employed for joint training and the resultant performance. The evaluation aims to investigate the effect of joint training by comparing the proposed 4D model with the CTC/RNN-T/attention (a three-decoder joint model), CTC/attention, and RNN-T models. To isolate the influence of joint training, the individual decoders are employed for decoding (i.e., CTC, attention, and RNN-T), avoiding the application of joint decoding. As depicted in Table III, WER significantly improves as the number of decoders used for joint training increases. This underscores the effectiveness of joint training using multiple decoders with distinct characteristics in effectively regularizing the encoder training.

3) *Limitation of joint training*: Table IV provides the training time for each model when training single and 4D models on the LibriSpeech 100 h dataset using NVIDIA A100 80GB

TABLE III
EFFECT OF THE NUMBER OF DECODERS DURING TRAINING ON LIBRISPEECH 100 H TEST-OTHER.

Joint training	Decoder	WER (↓)
CTC/Attention		20.66
CTC/RNN-T/Attn	CTC	20.56
CTC/RNN-T/Attn/MLM		18.96
CTC/Attention		19.43
CTC/RNN-T/Attn	Attention	18.70
CTC/RNN-T/Attn/MLM		17.91
RNN-T		18.30
CTC/RNN-T/Attn	RNN-T	18.34
CTC/RNN-T/Attn/MLM		17.61

TABLE IV
TRAINING TIMES.

Model	GPUs	GPU hours / epoch	Increase (↓)
CTC/Attn	1	0.16	1.0x
Mask-CTC	1	0.19	1.2x
RNN-T	2	0.86	5.5x
4D	4	1.40	8.9x

GPUs. RNN-T requires substantially more training time than the other two individual models (CTC/Attention and Mask-CTC) due to the considerable amount of GPU memory required for computing all possible RNN-T paths [18]. Because the 4D model incorporates four decoders, including the RNN-T decoder, the training time naturally increases (roughly the sum of the training times for each model).

However, during decoding, as long as a single decoder is utilized, there is no need for the forward computation of other decoders, ensuring that the decoding time remains comparable to that of the individual models (as further discussed in Section VI-C1). In addition, as mentioned in the Introduction, multiple models typically need to be trained for different application scenarios. Still, the 4D model offers the advantage of quickly switching between decoders. If three individual systems (CTC/attention, RNN-T, and Mask-CTC) need to be trained, the total training time would be 1.21 GPU hours / epoch, meaning that the increase in training time for the 4D model is only 16%.

C. Detailed analysis of the proposed one-pass beam search

This section provides a detailed analysis of joint decoding, specifically focusing on the RNN-T-driven one-pass beam search, demonstrating superior performance in Table I.

1) *Computational complexity of the beam search*: Figure 4 illustrates the relationship between the real-time factor (RTF) using a GPU (NVIDIA RTX3090) and WER on the LibriSpeech 100 h test-other set. The black dots denote the baselines, the blue dots represent 4D joint training but *without* one-pass beam search, and the green dots denote 4D joint training *with* RNN-T-driven one-pass beam search. In addition to the three-decoder one-pass beam search of CTC/RNN-T/attention, we show the results of the two-decoder one-pass beam search of CTC/RNN-T and RNN-T/attention. The decoding weights (μ_{ctc} , μ_{rnn} , μ_{att}) of the RNN-T-driven one-pass beam search in Algorithm 4 are (0.3, 0.7, 0.0) and (0.0, 0.5, 0.5) for CTC/RNN-T and RNN-T/attention, respectively.

Comparing the black and blue dots, the proposed 4D model consistently reduces WER for all decoders without an increase

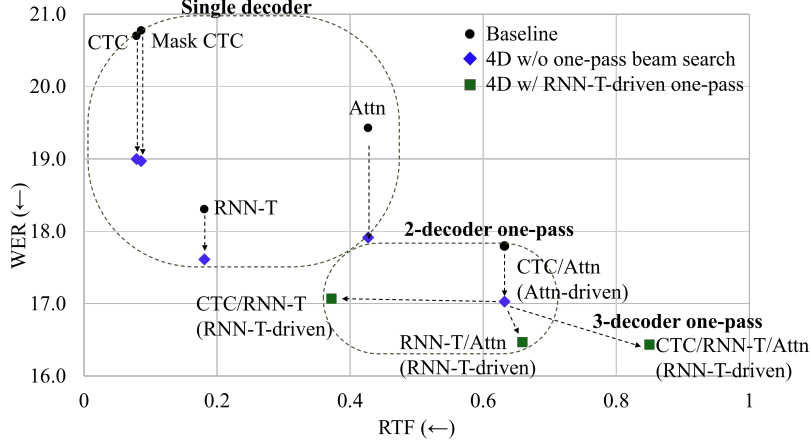


Fig. 4. Relationship between RTFs and WERs. The red, blue, and green dots represent the baselines, the 4D model without beam search, and the 4D model with beam search, respectively.

Ground truth	
ground truth: the hebreus were restive under this tyranny was natural inevitable	
Baseline (Attention-driven CTC/Attn)	
CTC: the heaps were restive under that ceremony was not really uncomfortable Attention: the heapers were arrestive under this journey was not tree inevitable CTC/Attn: the heapers were erective under this journey was not tree inevitable	
Proposed (RNN-T driven CTC/RNN-T/Attn)	
CTC: the heaps were restive under that ceremony was not really uncomfortable Attention: the heapers were arrestive under this journey was not tree inevitable RNN-T: the heaps were restive under that ceremony was not free inevitable CTC/RNN-T/Attn: the heapers were restive under this journey was not free inevitable	

Fig. 5. Typical examples of beam search results. Incorrect decoding results are highlighted in red. Conversely, correct decoding results are shown in blue, and results corrected by the joint decoding are further bolded.

in RTF. Although joint training requires more GPU memory and training time, as discussed in Section VI-B3, the proposed 4D model does not increase the decoding time as long as a single decoder is used.

Shifting the focus to joint decoding with two decoders, compared to conventional CTC/attention joint decoding (represented by the blue dot), CTC/RNN-T achieves a smaller RTF with a comparable WER, and RNN-T/attention achieves a better WER with a similar RTF. In addition, the three-decoder one-pass beam search of CTC/RNN-T/attention shows the best WER with a 30% larger RTF (0.85 vs. 0.65).

2) *Typical example of the joint decoding:* Figure 5 shows typical decoding results of the conventional CTC/attention and the proposed RNN-T driven one-pass beam search. The decoding results are also shown using each single decoder (CTC, attention, and RNN-T decoders). The incorrect decoding results are highlighted in red. Conversely, the correct decoding results are shown in blue, and results corrected by the joint decoding are further bolded. In both CTC/attention and the proposed one-pass beam search, joint decoding can correct the incorrectly decoded result if any decoder outputs a correct token. The proposed method integrates the three decoders, thereby enhancing the complementarity of each decoder resulting in a performance improvement in terms of WER.

3) *Effect of the decoding weights:* As depicted in Figure 6, we examine the effect of RNN-T weight μ_{rnn} by maintaining

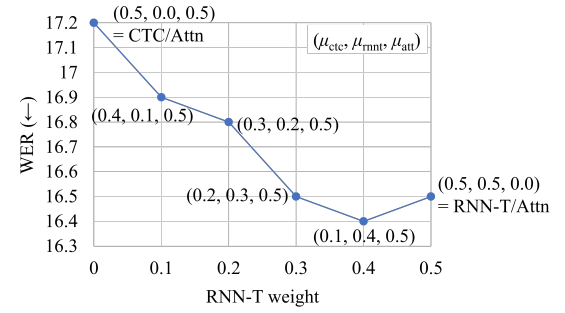


Fig. 6. Effect of the decoding weights. We tested the impact of the RNN-T weights by fixing the attention weight to 0.5 for CTC/attention. The proposed method consistently outperformed the baseline by increasing the RNN-T weight.

the attention weight μ_{att} at 0.5 for CTC/attention. The proposed method consistently outperforms the baseline by increasing the RNN-T weight, with the best performance observed when utilizing the decoding weights $(\mu_{\text{ctc}}, \mu_{\text{rnnt}}, \mu_{\text{att}}) = (0.1, 0.4, 0.5)$.

D. Comprehensive analysis of the one-pass beam search

This section provides a comprehensive analysis of the three proposed one-pass beam search algorithms in terms of WER-RTF tradeoff, decoder combination, and comparison with another joint decoding method.

1) *Comparison of the three one-pass beam search:* Figure 7 illustrates the relationship between the RTF using a GPU (NVIDIA RTX3090) and WER on the LibriSpeech 100 h test-other set. The black dots represent the baseline CTC/attention results, while the blue, red, and green dots represent the attention-driven, CTC-driven, and RNN-T-driven one-pass beam search, respectively. We also show the results for single-decoder and two-decoder one-pass beam search. The decoding weights $(\mu_{\text{ctc}}, \mu_{\text{rnnt}}, \mu_{\text{att}})$ for the two-decoder one-pass beam search in Algorithms 1, 3, and 4 are $(0.3, 0.7, 0.0)$, $(0.3, 0.0, 0.7)$, and $(0.0, 0.5, 0.5)$ for CTC/RNN-T, CTC/attention, and RNN-T/attention, respectively.

Upon comparison of the baseline with the three proposed one-pass beam search algorithms, all three methods exhibit

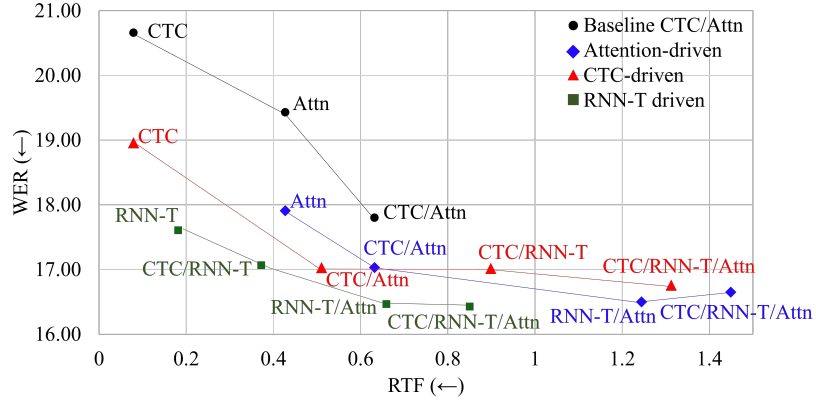


Fig. 7. Comparison of the three one-pass beam search methods. The black dots represent the conventional CTC/attention, while the red, blue, and green dots depict the results of the attention-driven, CTC-driven, and RNN-T-driven one-pass beam search results, respectively.

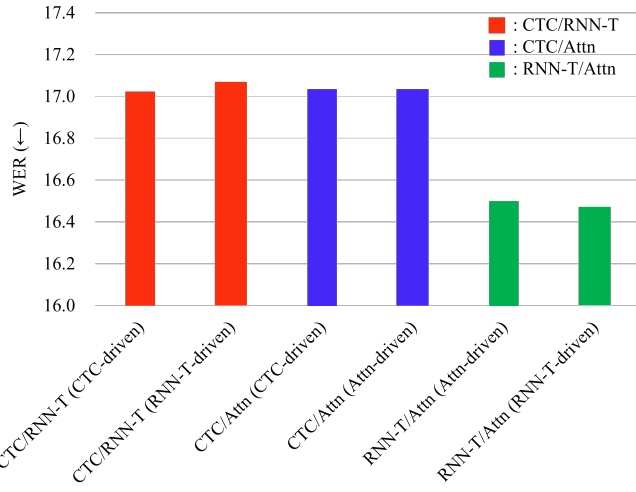


Fig. 8. Comparison of performance between different combinations of beam search strategies.

superior WER-RTF tradeoff curves, reflecting the improved baseline performance achieved through joint training. Analyzing the three proposed one-pass beam search algorithms, the RNN-T-driven method achieves the best WER-RTF tradeoff. This advantage stems from the fact that the CTC-driven and attention-driven methods compute all RNN-T paths through RNN-T prefix scoring, whereas the RNN-T-driven one-pass beam search avoids this computation.

2) *Analysis of different decoder combinations:* Figure 8 shows the performance when using two of the CTC, RNN-T, and attention decoders (CTC/RNN-T, CTC/attention, RNN-T/attention). A total of six different combinations are compared, depending on which decoder is designated as the primary decoder. Interestingly, regardless of the primary decoder, when the decoder used for joint scoring is the same, the performance is nearly comparable. Within this experimental setting, the RNN-T/attention combination exhibits the lowest WER. This result is primarily attributed to the inherent performance capabilities of each decoder. Considering the WER-RTF tradeoff shown in Figure 7, the proposed method can switch between decoders to show reasonable performance with smaller RTFs for different application scenarios.

TABLE V
WER COMPARISON: ONE-PASS BEAM SEARCH VS. ROVER ON LIBRISPEECH 100 H.

Decoding method	test-clean	test-other
Attn-driven CTC/RNN-T/Att	6.5	16.6
CTC-driven CTC/RNN-T/Att	6.3	16.8
RNN-T-driven CTC/RNN-T/Att	6.3	16.4
ROVER (CTC/RNN-T/Att)	6.3	16.6
ROVER (CTC/RNN-T/Att/Mask-CTC)	6.4	16.8

3) *Comparison of performance with ROVER:* In addition, we compare the proposed one-pass beam search method with the recognizer output voting error reduction method (ROVER) [57] in Table V. Overall, ROVER and the three proposed one-pass beam search algorithms show almost equal WER, but the RNN-T-driven one-pass beam search shows the best WER. Although ROVER is a powerful method, it increases system complexity and computation time because it requires complete token sequences from all decoders for integration. In contrast, the proposed method is more efficient because the secondary decoders do not need to generate complete token sequences.

VII. DISCUSSION

Summarizing the findings from Section VI, several key observations emerge: 1) performance improves with an increasing number of decoders used for joint training (Section VI-B2). 2) A larger number of decoders employed for joint decoding enhances performance, as reflected in the WER-RTF tradeoff (Section VI-C1). 3) Notably, the RNN-T-driven one-pass beam search demonstrates a superior WER-RTF tradeoff compared to other joint decoding methods, including CTC-driven and attention-driven as well as the baseline CTC/attention curves (Section VI-D).

An inherent advantage of the 4D model lies in its ability to switch between decoders depending on the application scenario. Despite the increased training and decoding time associated with joint training and decoding, this model eliminates the need for training a different model for each application. Moreover, depending on the application scenario, it allows one to choose an appropriate decoding algorithm, such as a two-decoder or three-decoder one-pass beam search. For example, the CTC decoder is appropriate for real-time

processing with limited computational resources. In contrast, the one-pass beam search with three decoders becomes viable when sufficient computational resources are available. Considering these attributes, the proposed 4D model is a practical system capable of achieving a superior WER-RTF tradeoff curve compared to the baseline CTC/attention.

VIII. CONCLUSION

This paper introduces a 4D joint model incorporating CTC, attention, RNN-T, and Mask-CTC, with a shared encoder trained through multitask learning. The study demonstrates the efficacy of jointly trained 4D models, employing a two-stage training strategy that enhances the performance of individual decoders. Notably, the proposed joint CTC/RNN-T/attention decoding exhibits improved performance, surpassing the previously proposed CTC/attention decoding. The RNN-T-driven one-pass beam search, in particular, showcases a superior WER-RTF tradeoff compared to other joint decoding methods, including CTC-driven, attention-driven one-pass beam search algorithms, and the baseline CTC/attention curves.

REFERENCES

- [1] R. Prabhavalkar, T. Hori, T. N. Sainath, R. Schluter, and S. Watanabe, “End-to-end speech recognition: A survey,” *IEEE/ACM Transactions on Audio, Speech, and Language Processing*, vol. 32, pp. 325–351, 2023.
- [2] J. Li, “Recent advances in end-to-end automatic speech recognition,” *APSIPA Transactions on Signal and Information Processing*, vol. 11, no. 1, 2022.
- [3] A. Graves, S. Fernández, F. Gomez, and J. Schmidhuber, “Connectionist temporal classification: Labelling unsegmented sequence data with recurrent neural networks,” in *International Conference on Machine Learning (ICML)*, 2006, pp. 369–376.
- [4] A. Graves and N. Jaitly, “Towards end-to-end speech recognition with recurrent neural networks,” in *International Conference on Machine Learning (ICML)*, 2014, pp. 1764–1772.
- [5] S. Kriman, S. Beliaev, B. Ginsburg, J. Huang, O. Kuchaiev, V. Lavrukhin, R. Leary, J. Li, and Y. Zhang, “Quartznet: Deep automatic speech recognition with 1d time-channel separable convolutions,” in *IEEE International Conference on Acoustics, Speech, and Signal Processing (ICASSP)*, 2020, pp. 6124–6128.
- [6] A. Graves, “Sequence transduction with recurrent neural networks,” in *International Conference on Machine Learning (ICML)*, 2012.
- [7] Q. Zhang, H. Lu, H. Sak, A. Tripathi, E. McDermott, S. Koo, and S. Kumar, “Transformer transducer: A streamable speech recognition model with transformer encoders and rnn-t loss,” in *IEEE International Conference on Acoustics, Speech, and Signal Processing (ICASSP)*, 2020, pp. 7829–7833.
- [8] W. Han, Z. Zhang, Y. Zhang, J. Yu, C.-C. Chiu, J. Qin, A. Gulati, R. Pang, and Y. Wu, “Contextnet: Improving convolutional neural networks for automatic speech recognition with global context,” in *Interspeech*, 2020, pp. 3610–3614.
- [9] K. Rao, H. Sak, and R. Prabhavalkar, “Exploring architectures, data and units for streaming end-to-end speech recognition with RNN-transducer,” in *IEEE Workshop on Automatic Speech Recognition and Understanding (ASRU)*, 2017, pp. 193–199.
- [10] W. Chan, N. Jaitly, Q. Le, and O. Vinyals, “Listen, attend and spell: A neural network for large vocabulary conversational speech recognition,” in *IEEE International Conference on Acoustics, Speech, and Signal Processing (ICASSP)*, 2016, pp. 4960–4964.
- [11] J. K. Chorowski, D. Bahdanau, D. Serdyuk, K. Cho, and Y. Bengio, “Attention-based models for speech recognition,” in *Advances in Neural Information Processing Systems (NeurIPS)*, vol. 28, 2015, pp. 577–585.
- [12] S. Karita, N. Chen, T. Hayashi, T. Hori, H. Inaguma, Z. Jiang, M. Someki, N. E. Y. Soplin, R. Yamamoto, X. Wang *et al.*, “A comparative study on transformer vs rnn in speech applications,” in *IEEE Workshop on Automatic Speech Recognition and Understanding (ASRU)*, 2019, pp. 449–456.
- [13] P. Guo, F. Boyer, X. Chang, T. Hayashi, Y. Higuchi, H. Inaguma, N. Kamo, C. Li, D. Garcia-Romero, J. Shi *et al.*, “Recent developments on espnet toolkit boosted by conformer,” in *IEEE International Conference on Acoustics, Speech, and Signal Processing (ICASSP)*, 2021, pp. 5874–5878.
- [14] Y. Higuchi, S. Watanabe, N. Chen, T. Ogawa, and T. Kobayashi, “Mask ctc: Non-autoregressive end-to-end asr with ctc and mask predict,” in *Interspeech*, 2020, pp. 3655–3659.
- [15] N. Chen, S. Watanabe, J. Villalba, P. Źelasko, and N. Dehak, “Non-autoregressive transformer for speech recognition,” *IEEE Signal Processing Letters*, vol. 28, pp. 121–125, 2020.
- [16] X. Song, Z. Wu, Y. Huang, C. Weng, D. Su, and H. Meng, “Non-autoregressive transformer asr with ctc-enhanced decoder input,” in *IEEE International Conference on Acoustics, Speech, and Signal Processing (ICASSP)*, 2021, pp. 5894–5898.
- [17] L. Kürzinger, D. Winkelbauer, L. Li, T. Watzel, and G. Rigoll, “Ctc-segmentation of large corpora for german end-to-end speech recognition,” in *Speech and Computer*, A. Karpov and R. Potapova, Eds. Cham: Springer International Publishing, 2020, pp. 267–278.
- [18] F. Kuang, L. Guo, W. Kang, L. Lin, M. Luo, Z. Yao, and D. Povey, “Pruned RNN-T for fast, memory-efficient ASR training,” in *Interspeech*, 2022, pp. 2068–2072.
- [19] D. Bahdanau, K. Cho, and Y. Bengio, “Neural machine translation by jointly learning to align and translate,” in *International Conference on Learning Representations (ICLR)*, 2015.
- [20] A. Radford, J. W. Kim, T. Xu, G. Brockman, C. McLeavey, and I. Sutskever, “Robust speech recognition via large-scale weak supervision,” in *International Conference on Machine Learning (ICML)*, vol. 202. PMLR, 2023, pp. 28492–28518.
- [21] S. Watanabe, T. Hori, S. Kim, J. R. Hershey, and T. Hayashi, “Hybrid ctc/attention architecture for end-to-end speech recognition,” *IEEE Journal of Selected Topics in Signal Processing*, vol. 11, no. 8, pp. 1240–1253, 2017.
- [22] M. Ghazvininejad, O. Levy, Y. Liu, and L. Zettlemoyer, “Mask-predict: Parallel decoding of conditional masked language models,” in *Proc. EMNLP-IJCNLP*, 2019.
- [23] H. Futami, H. Inaguma, S. Ueno, M. Mimura, S. Sakai, and T. Kawahara, “Non-autoregressive error correction for ctc-based asr with phone-conditioned masked lm,” in *Interspeech*, 2022, pp. 3889–3893.
- [24] S. Ueno, H. Inaguma, M. Mimura, and T. Kawahara, “Acoustic-to-word attention-based model complemented with character-level ctc-based model,” in *IEEE International Conference on Acoustics, Speech, and Signal Processing (ICASSP)*, 2018, pp. 5804–5808.
- [25] T. Nakatani, “Improving transformer-based end-to-end speech recognition with connectionist temporal classification and language model integration,” in *Interspeech*, 2019.
- [26] Y. Peng, J. Tian, B. Yan, D. Berrebbi, X. Chang, X. Li, J. Shi, S. Arora, W. Chen, R. Sharma *et al.*, “Reproducing whisper-style training using an open-source toolkit and publicly available data,” in *IEEE Workshop on Automatic Speech Recognition and Understanding (ASRU)*, 2023, pp. 1–8.
- [27] Y. Peng, J. Tian, W. Chen, S. Arora, B. Yan, Y. Sudo, S. Muhammad, K. Choi, J. Shi, X. Chang *et al.*, “OWSM v3.1: Better and faster open whisper-style speech models based on E-Branchformer,” *arXiv preprint arXiv:2401.16658*, 2024.
- [28] B. Zhang, H. Lv, P. Guo, Q. Shao, C. Yang, L. Xie, X. Xu, H. Bu, X. Chen, C. Zeng *et al.*, “Wenetspeech: A 10000+ hours multi-domain mandarin corpus for speech recognition,” in *IEEE International Conference on Acoustics, Speech, and Signal Processing (ICASSP)*, 2022, pp. 6182–6186.
- [29] Y. Yin, D. Mori, and S. Fujimoto, “Reazonspeech: A free and massive corpus for japanese asr,” in *The Association for Natural Language Processing*, 2023, pp. 1134–1139.
- [30] T. N. Sainath, R. Pang, D. Rybach, Y. He, R. Prabhavalkar, W. Li, M. Visontai, Q. Liang, T. Strohman, Y. Wu *et al.*, “Two-pass end-to-end speech recognition,” in *Interspeech*, 2019, pp. 2713–2777.
- [31] K. Hu, T. N. Sainath, R. Pang, and R. Prabhavalkar, “Deliberation model based two-pass end-to-end speech recognition,” in *IEEE International Conference on Acoustics, Speech, and Signal Processing (ICASSP)*. IEEE, 2020, pp. 7799–7803.
- [32] K. Hu, R. Pang, T. N. Sainath, and T. Strohman, “Transformer based deliberation for two-pass speech recognition,” in *IEEE Spoken Language Technology Workshop (SLT)*, 2021, pp. 68–74.
- [33] Z. Tian, J. Yi, J. Tao, S. Zhang, and Z. Wen, “Hybrid autoregressive and non-autoregressive transformer models for speech recognition,” *IEEE Signal Processing Letters*, vol. 29, pp. 762–766, 2022.

[34] W. Wang, K. Hu, and T. N. Sainath, “Deliberation of streaming rnn transducer by non-autoregressive decoding,” in *IEEE International Conference on Acoustics, Speech, and Signal Processing (ICASSP)*, 2022, pp. 7452–7456.

[35] Z. Yao, D. Wu, X. Wang, B. Zhang, F. Yu, C. Yang, Z. Peng, X. Chen, L. Xie, and X. Lei, “Wenet: Production oriented streaming and non-streaming end-to-end speech recognition toolkit,” in *Interspeech*, 2021, pp. 4045–4058.

[36] A. Narayanan, T. N. Sainath, R. Pang, J. Yu, C.-C. Chiu, R. Prabhavalkar, E. Variani, and T. Strohman, “Cascaded encoders for unifying streaming and non-streaming asr,” in *IEEE International Conference on Acoustics, Speech, and Signal Processing (ICASSP)*, 2020, pp. 5629–5633.

[37] J. Mahadeokar, Y. Shi, K. Li, D. Le, J. Zhu, V. Chandra, O. Kalinli, and M. L. Seltzer, “Streaming parallel transducer beam search with fast-slow cascaded encoders,” in *Interspeech*, 2022, pp. 2083–2087.

[38] K. Li, J. Mahadeokar, J. Guo, Y. Shi, G. Keren, O. Kalinli, M. L. Seltzer, and D. Le, “Improving fast-slow encoder based transducer with streaming deliberation,” *IEEE International Conference on Acoustics, Speech, and Signal Processing (ICASSP)*, pp. 1–5, 2023.

[39] J. Yu, W. Han, A. Gulati, C.-C. Chiu, B. Li, T. N. Sainath, Y. Wu, and R. Pang, “Dual-mode ASR: Unify and improve streaming ASR with full-context modeling,” in *International Conference on Learning Representations (ICLR)*, 2021.

[40] N. Moritz, T. Hori, and J. L. Roux, “Dual causal/non-causal self-attention for streaming end-to-end speech recognition,” in *Interspeech*, 2021, pp. 1822–1826.

[41] F. Weninger, M. Gaudesi, M. A. Haidar, N. Ferri, J. Andrés-Ferrer, and P. Zhan, “Conformer with dual-mode chunked attention for joint online and offline asr,” in *Interspeech*, 2022, pp. 2053–2057.

[42] B. Yan, S. Dalmia, Y. Higuchi, G. Neubig, F. Metze, A. W. Black, and S. Watanabe, “Ctc alignments improve autoregressive translation,” in *Proceedings of the 17th Conference of the European Chapter of the Association for Computational Linguistics*, 2022, pp. 1623–1639.

[43] E. Tsunoo, H. Futami, Y. Kashiwagi, S. Arora, and S. Watanabe, “Integration of Frame- and Label-synchronous Beam Search for Streaming Encoder-decoder Speech Recognition,” in *Interspeech*, 2023, pp. 1369–1373.

[44] Y. Sudo, S. Muhammad, Y. Peng, and S. Watanabe, “Time-synchronous one-pass Beam Search for Parallel Online and Offline Transducers with Dynamic Block Training,” in *Interspeech*, 2023, pp. 4479–4483.

[45] Y. Sudo, S. Muhammad, B. Yan, J. Shi, and S. Watanabe, “4D ASR: Joint modeling of CTC, attention, transducer, and mask-predict decoders,” in *Interspeech*, 2023, pp. 3312–3316.

[46] A. Gulati, C. Chiu, J. Qin, J. Yu, N. Parmar, R. Pang, S. Wang, W. Han, Y. Wu, Y. Zhang, and Z. Zhang, “Conformer: Convolution-augmented transformer for speech recognition,” in *Interspeech*, 2020, pp. 5036–5040.

[47] J. L. Ba, J. R. Kiros, and G. E. Hinton, “Layer normalization,” *Advances in Neural Information Processing Systems (NeurIPS)*, 2016.

[48] K. He, X. Zhang, S. Ren, and J. Sun, “Deep residual learning for image recognition,” in *The IEEE/CVF Conference on Computer Vision and Pattern Recognition (CVPR)*, 2016, pp. 770–778.

[49] X. Lin, H. S. Baweja, G. A. Kantor, and D. Held, “Adaptive auxiliary task weighting for reinforcement learning,” in *Advances in Neural Information Processing Systems (NeurIPS)*, 2019.

[50] N. Moritz, T. Hori, and J. Le Roux, “Triggered attention for end-to-end speech recognition,” in *IEEE International Conference on Acoustics, Speech, and Signal Processing (ICASSP)*, 2019, pp. 5666–5670.

[51] D. S. Park, W. Chan, Y. Zhang, C. Chiu, B. Zoph, E. D. Cubuk, and Q. V. Le, “SpecAugment: A simple data augmentation method for automatic speech recognition,” in *Interspeech*, 2019, pp. 2613–2617.

[52] D. P. Kingma and J. Ba, “Adam: A method for stochastic optimization,” *CoRR*, vol. abs/1412.6980, 2015.

[53] V. Panayotov, G. Chen, D. Povey, and S. Khudanpur, “Librispeech: an asr corpus based on public domain audio books,” in *IEEE International Conference on Acoustics, Speech, and Signal Processing (ICASSP)*, 2015, pp. 5206–5210.

[54] K. Maekawa, “Corpus of spontaneous Japanese: Its design and evaluation,” in *ISCA/IEEE Workshop on Spontaneous Speech Processing and Recognition*, 2003.

[55] A. Kurematsu, K. Takeda, Y. Sagisaka, S. Katagiri, H. Kuwabara, and K. Shikano, “Atr japanese speech database as a tool of speech recognition and synthesis,” *Speech Communication*, vol. 9, no. 4, pp. 357–363, 1990.

[56] S. Watanabe, T. Hori, S. Karita, T. Hayashi, J. Nishitoba, Y. Unno, N. Enrique Yalta Soplin, J. Heymann, M. Wiesner, N. Chen, A. Renduchintala, and T. Ochiai, “ESPnet: End-to-end speech processing toolkit,” in *Interspeech*, 2018, pp. 2207–2211.

[57] J. G. Fiscus, “A post-processing system to yield reduced word error rates: Recognizer output voting error reduction (rover),” in *IEEE Workshop on Automatic Speech Recognition and Understanding (ASRU)*, 1997, pp. 347–354.